Herschel Planetary Nebula Survey (HerPlaNS)

Toshiya Ueta,[1,2,3] Djazia Ladjal,[1] Katrina Exter,[4] Masaaki Otsuka,[5] and the HerPlaNS team

[1]*Department of Physics & Astronomy, University of Denver, USA*
[2]*Institute of Space and Astronautical Science, JAXA, Japan*
[3]*Japan Society for the Promotion of Science Long-Term Invitation Fellow*
[4]*Institute of Astronomy, KU Leuven, Belgium*
[5]*Academia Sinica Institute of Astronomy and Astrophysics, Taiwan*

ABSTRACT

Herschel Planetary Nebula Survey (HerPlaNS) is a far-IR imaging and spectroscopic survey of planetary nebulae, performed with the *Herschel Space Observatory*, aiming at understanding the energetics and shaping history of the circumstellar nebulae. Below we briefly demonstrate the breadth and depth of the HerPlaNS data set using one of the targets, NGC 6781, as an example, and explore expectations in the era of *SPICA*, the next-generation far-IR mission.

1. HERSCHEL PLANETARY NEBULA SURVEY (HERPLANS)

The Herschel Planetary Nebula Survey (HerPlaNS) is an open-time program of the *Herschel Space Observatory* (Pilbratt et al. 2010) conducted by a team of about 30 astronomers.[1] Our chief objective is to examine the spatially-resolved far-IR characteristics of planetary nebulae (PNs; Table 1) as energetic systems of gas and dust by mustering the telescope's mapping and spectroscopic capabilities. Far-IR observations allow simultaneous probing of the dust component via thermal continuum emission and the gas component via far-IR fine-structure and molecular line emission without much extinction. The spatially-resolved energetics as a function of location in these nebulae will provide more insights about the evolution of the central star and circumstellar shells. In this contribution, we present a brief overview of the survey and its data products, summarizing the potential of the data set using NGC 6781 as an example (§2), and hint at expectations for the era of *SPICA* (§3). A complete account of the present summary is found elsewhere (Ueta et al. 2014).

2. HERPLANS DATA DEMONSTRATION WITH NGC 6781

Table 1. List of HerPlaNS Target PNs

Name	PN G	Morph[a]	D (kpc)	R (pc)	Age (10^3 yr)	T_* (10^3 K)	H_2	X-Rays[b]
NGC 40	120.0+09.8	Bbsh	1.0	0.11	4	48	N	D
NGC 2392	197.8+17.3	Rsai	1.3	0.14	3	47	N	D, P
NGC 3242	261.0+32.0	Ecspaih	1.0	0.10	4	89	N	D
NGC 6445	008.0+03.9	Mpi	1.4	0.14	3	170	Y	P
NGC 6543	096.4+29.9	Mcspa	1.5	0.09	5	48	N	D, P
NGC 6720	063.1+13.9	Ecsh	0.7	0.13	6	148	Y	N
NGC 6781	041.8−02.9	Bth	1.0	0.32	26	112	Y	N
NGC 6826	083.5+12.7	Ecsah	1.3	0.08	5	50	N	D, P
NGC 7009	037.7−34.5	Lbspa	1.5	0.09	3	87	N	D, P
NGC 7026[c]	089.0+00.3	Bs	1.7	0.16	< 1	80	N	D, P?
Mz 3[d]	331.7−01.0	Bps	1–3	0.1–0.2	0.6–2	32:	Y	D, P

(a) According to the morphological classification by Sahai et al. (2011). (b) The HerPlaNS sample is a subset of the Chandra X-ray Planetary Nebula Survey (Kastner et al. 2012): D - diffuse, P - point-source X-ray detection. (c) Not a ChanPlaNS target PN; data from Gruendl et al. (2006). The PSF of XMM-Newton does not allow clear determination of the presence of a point source. (d) Not a ChanPlaNS target PN; may be a symbiotic/PN mimic (Frew 2008); data from Kastner et al. (2003).

[1] The founding members are T. Ueta, D. Ladjal (DU), K. M. Exter (KUL), M. Otsuka (ASIAA), R. Szczerba, N. Siódmiak (NCAC), I. Aleman, A. G. G. M. Tielens (Leiden U.) J. H. Kastner, J. Nordhaus (RIT), R. Montez (Vanderbilt), I. McDonald, K. Hebden, A. Zijlstra (U. of Manchester), M. Wittkowski (ESO), S. Ramstedt (Uppsala U.), O. De Marco (Macquarie U.), E. Villaver (UAM), B. Balick (UW), E. Behar (Technion), E. G. Blackman (U. of Rochester, Y.-H. Chu (UIUC), J. L. Hora (CfA/Harvard), H. Izumiura (OAO/NAOJ), J. A. Lopez (UNAM), K. Murakawa (Leeds), R. Nordon (MPE), C. Sandin (AIP), R. Sahai (JPL), P. A. M. van Hoof (KSB/ORB), W. Vlemmings (Chalmers), and I. Yamamura (ISAS/JAXA).

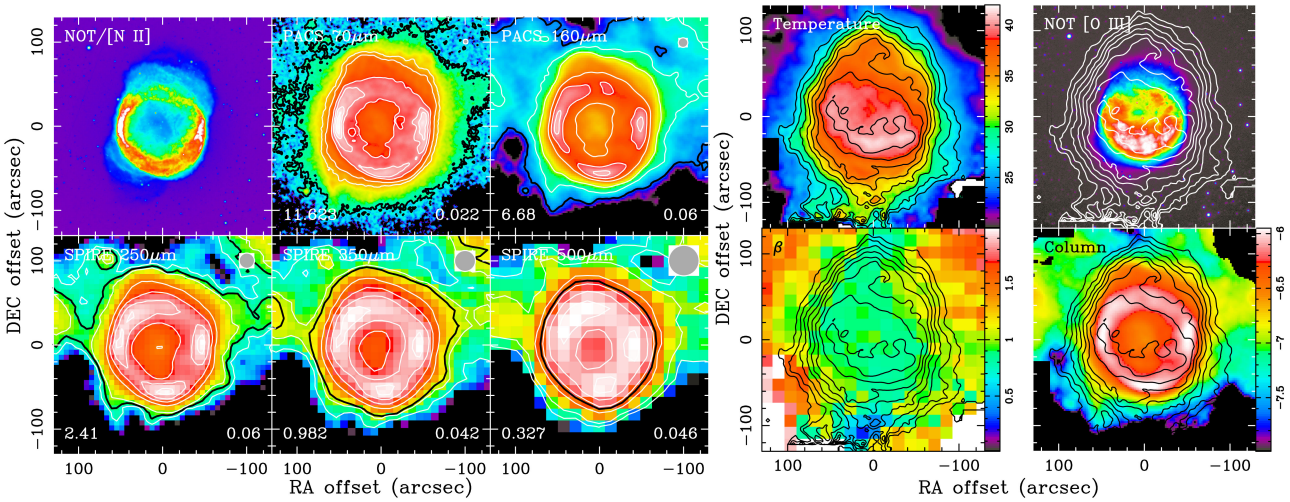

Figure 1. (*Left*:) HerPlaNS broadband far-IR images of NGC 6781 with an [N II] image taken at the Nordic Optical Telescope (NOT; Phillips et al. 2011). The far-IR peak surface brightness and 1-σ sky noise in mJy arcsec^{-2} are indicated at the bottom-left and right corners, respectively. At the top-right corner, the beam is shown: 5.″61, 11.″39, 18.″2, 24.″9, and 36.″3, respectively. Contours are 90, 70, 50, 30, 10, and 5 % of the peak, and the black contour indicates 3-σ threshold. The pixel scales are 1, 1, 2, 6, 9, and 14 arcsec pix^{-1}, respectively, from top left to bottom right. (*Top Left*) The dust temperature ($T_{\rm dust}$) map of NGC 6781 at the 11.″4 resolution derived by a power-law dust emissivity fit. The peak is 41.3 K, with contours at a 2 K interval from 40 to 26 K. These $T_{\rm dust}$ contours are always overlaid in other frames. (*Top Right*) the NOT [O III] λ5007 map showing the high-ionization regions. (*Bottom Left*) The power-law index (β) map at the 36.″3 resolution. (*Bottom Right*) The dust column mass density ($M_\odot$ pix^{-1}) map at the 11.″4 resolution.

NGC 6781 is a PN near the end of the interior nuclear burning phase, whose central star (CSPN) is of 110 kK (Frew 2008) and 385 $L_\odot$ at 950 ± 143 pc away (Schwarz & Monteiro 2006). Comparison of these parameters with evolutionary tracks of Vassiliadis & Wood (1994) suggests that the initial and present masses of the central star are 1.5 and 0.6 $M_\odot$, respectively, and the age of the PN since the AGB turn-off is 3×10^4 yr.

The optical nebula of NGC 6781 shows a signature "ring" of 50″radius within a diffuse, low-emission nebula extending 190″×160″ (Mavromatakis et al. 2001; Phillips et al. 2011). Morpho-kinematic observations in molecular lines (Bachiller et al. 1993; Hiriart 2005) indicated that the nebula is a nearly pole-on cylinder with an equatorial enhancement (i.e., barrel) with the 4×10^4 yr dynamical age at adopted 950 pc.

Hence, the spatially-resolved data of NGC 6781 will reveal variations nebular quantities in the equatorial plane as a function of radius, taking into account the height of the bipolar structure along the direction of the line of sight.

2.1. **Broadband Imaging: Diagnostics via Dust Continuum**

HerPlaNS broadband imaging consists of PACS dual-band imaging at 70 and 160 μm over a 600″ × 600″ field and SPIRE triple-band imaging at 250, 350, and 500 μm over a 240″ × 480″ field. Far-IR images of NGC 6781 (Figure 1, left) reveal the signature ring of the near pole-on cylindrical barrel in all five far-IR bands. The total fluxes are measured by aperture photometry with the 3-$\sigma_{\rm sky}$ threshold (Table 2).

The surface brightness distribution at 70 μm is co-spatial with low-ionization optical line emission. The emission peaks at the eastern and western rims represent the pivot points of the inclined barrel. The brighter southern rim shows the higher-temperature inner barrel wall in the cavity, while the dimmer northern rim shows the lower-temperature outer barrel wall. This surface brightness imbalance becomes less at longer wavelengths where the optical depth is low and the "ring"

Table 2. Far-IR Image Characteristics and Photometry of NGC 6781

Band	λ (μm)	$\Delta\lambda$ (μm)	$I_{\rm peak}$ (mJy arcsec^{-2})	$\sigma_{\rm sky}$ (mJy arcsec^{-2})	F_ν (Jy)
PACS Blue	70	25	11.623	0.022	65.42 ± 3.28
PACS Red	160	85	6.68	0.06	64.88 ± 3.28
SPIRE PSW	250	76	2.41	0.06	30.04 ± 4.60
SPIRE PMW	350	103	0.982	0.042	14.56 ± 2.25
SPIRE PLW	500	200	0.327	0.046	6.41 ± 1.02

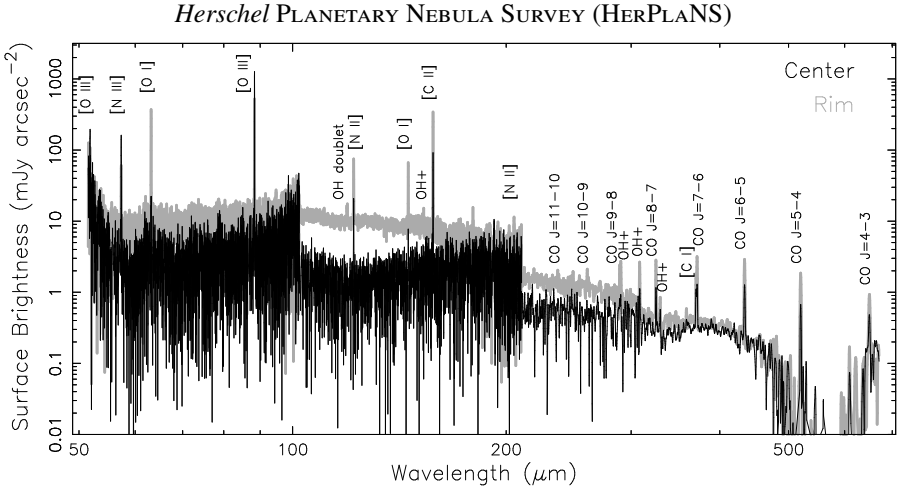

Figure 2. Spectra of NGC 6781 over the entire 51–672 μm coverage at the "center" (*black line*) and on the eastern "rim" (*gray line*) of the nebula. The flux units are set to show the surface brightness (mJy arcsec^{-2}) at these specific positions.

looks more complete. The extent of the far-IR emission is about the same as the diffuse [N II] emission of a deep exposure image (about 100″radius at 5-σ; Mavromatakis et al. 2001). Hence, the diffuse line emission is probably caused by dust grains scattering the line emission.

By fitting these emission maps with the power-law dust emissivity ($S_\nu \propto \lambda^{-\beta} B_\nu(T_{\rm dust})$, where β is the emissivity index and $T_{\rm dust}$ is the temperature), we successively derive the β, $T_{\rm dust}$, optical depth, and dust column mass density maps (Figure 1, right). The high $T_{\rm dust}$ region ($\gtrsim$ 40 K) is co-spatial with the [O III] λ5007 line emission, delineating the inner highly-ionized region of barrel wall directly visible to us. The β map is almost entirely unity, suggesting that the far-IR emitting dust is carbon-based (Volk & Kwok 1988), which is consistent with the previous optical line abundance analyses (Liu et al. 2004b) and the absence of silicate dust features in the mid-IR spectra (e.g., Phillips et al. 2011).

Because far-IR thermal dust continuum is optically thin ($\tau_{160\,\mu{\rm m}} = 10^{-5}$ to 10^{-6} on the "ring"), the dust column mass density map probes the whole nebula depth along the line of sight, corroborating the pole-on barrel structure previously only inferred and modeled with optical data. By integrating over the entire nebula, the total amount of far-IR emitting dust is determined to be $M_{\rm dust} = 3.8 \times 10^{-3}\,{\rm M}_\odot$ and roughly 50 % of this mass seems to be contained in the cylindrical barrel.

2.2. **Spatio-Spectroscopy: Diagnostics via Gas Emission**

HerPlaNS spectroscopy includes PACS integral-field-unit range-scan spectroscopy in the B2A band (51–72 μm), B2B band (70–105 μm), and R1 bands (103–145 μm and 140–220 μm), achieving the spectral coverage of 51–220 μm resulting in 25 spectra over a 47″×47″ field and SPIRE Fourier-transform spectrometer spectroscopy to cover 194–672 μm resulting in 35 spectra in the SSW band (194–313 μm) and 19 spectra in the SLW band (303–672 μm) sparsely sampled over a field of a ∼ 120″ radius.

Figure 2 shows spectra for the whole 51–672 μm at two spatial pointings (at the center and eastern rim). At both pointings, continuum is detected at about $\lesssim$10 mJy arcsec^{-2} in the PACS range and less than a few mJy arcsec^{-2} in the SPIRE range. Thermal dust continuum emission in the PACS range is generally stronger at the eastern rim, but is about the same at both pointings in the SPIRE range. This indicates that the central highly-ionized barrel cavity is completely surrounded by a colder dusty envelope.

Besides continuum, a number of ionic and atomic lines in the PACS range, and a number of CO rotational transitions and other molecular species are seen in the SPIRE range. The relative line strengths of the two pointings suggest that the central cavity is more strongly ionized. While rich in lines, we determine that line contamination in broadband mapping is less than 5 % based on these spectra.

Moreover, PACS/SPIRE spectra taken by arrays of spaxels/bolometers can be rendered into spectral line maps by integrating the data cube over specific emission lines (Figure 3). Such line maps provide us with a new means to perform far-IR line diagnostics in a spatially-resolved manner and constrain the physical stratification of the medium. In the case of NGC 6781, two pointings are adjacent to each other, and hence, a single mosaic map covering most of the mid-section of the nebula can be recovered.

Using far-IR line ratio maps (e.g., [O III] 52 μm/88 μm and [N II] 122 μm/205 μm) augmented with other optical-to-far-IR line ratio maps (e.g., [O III] λ5007/88 μm and [N II] λ6583/122 μm), the electron temperature ($T_{\rm e}$) and electron density ($n_{\rm e}$) maps can be derived by solving the equation of statistical equilibrium for the lowest several excitation levels of these atoms (Liu et al. 2001, 2004a,b). Moreover, these ($T_{\rm e}$, $n_{\rm e}$) maps can be translated into ionic/elemental abundance maps with various ionization correction factors (Liu et al. 2001; Vamvatira-Nakou et al. 2013). For NGC 6781, we collapsed these maps into 1-D profiles along the RA direction in the end (Figure 3).

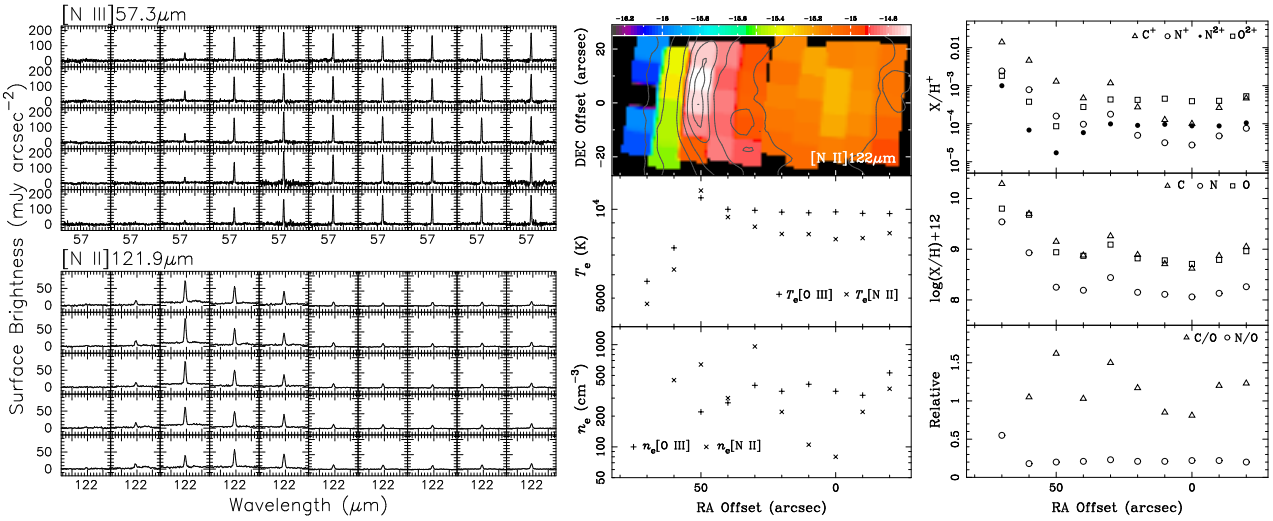

Figure 3. (*Left*) Spatial variation of [N III] 57 μm (*top*) and [N II] 122 μm (*bottom*) line emission in individual spectra. (*Middle*) The [N II] 122 μm line intensity map (*top in hue*). The log T_e profiles (*middle*). The log n_e profiles (*bottom*). (*Right*) The relative ionic abundance profiles (*top*). The relative elemental abundance profiles (where log N_H = 12; *middle*). The C/O and N/O profiles (*bottom*). The legend is given in each frame — *Crosses*: T_e, n_e based on [O III], *Pluses*: T_e, n_e based on [N II], *Triangles*: C^+, log(C/H) + 12, and C/O, *Circles*: N^+ (*open*), N^{2+} (*filled*), log(N/H) + 12, and N/O, *Squares*: O^{2+} and log(O/H) + 12.

The T_e profiles reveals constant T_e (~9,000 K) in the highly-ionized barrel cavity, surrounded by the T_e maximum (~10,500 K) beyond which T_e tapers off. The n_e profiles show a high-ionization gas n_e[O III] at constant (*pluses*; ~400 cm^{-3}) and a low-ionization gas n_e[N II] with a radially increasing trend (*crosses*; 100–600 cm^{-3}).

The ionic abundance profiles reveal the physical stratification: the highly ionized cavity ($\lesssim$30″) in which energetic photons ionize O^+ (> 35.12 eV), the inner barrel wall (between 30″and 40″) where still energetic photons ionize N^+ (>29.60 eV), and the barrel wall peak and beyond ($\gtrsim$50″) where only less energetic photons ionize N^0 and C^0 (<29.60 eV). There should be photo-dissociation regions farther out, but they are not detected in the present data. If they were, we could have performed similar line diagnostics exclusively for the photo-dissociation regions with surface brightness maps in neutral N ([N I] λ5199,5202) and in neutral H (H I at 21 cm), for example.

The CNO elemental abundances are roughly the same. The average elemental abundances relative to H are 8.9 for C, 8.2 for N, and 8.9 for O (0.5, 0.4, and 0.2 dex more than solar, respectively; Grevesse et al. 2010). The marginal N overabundance disqualifies NGC 6781 from being Peimbert Type I (N/O $\gtrsim$ 0.5; Peimbert & Torres-Peimbert 1983), i.e., the CSPN is less than 2 $M_\odot$ initial mass. The C-rich stellar ejecta appear to be accumulating at the barrel wall: the rise of C/O near the wall does not seem to reflect the evolutionary epoch where C becomes more abundant in the CSPN.

3. EXPECTATIONS FOR THE ERA OF *SPICA*

As briefly reviewed, spatially-resolved far-IR data from *Herschel* have just enabled us to decipher the physical stratifications in relatively isolated dusty gaseous systems. These insights will enhance the understanding of not only the PN physics itself but also the general far-IR line diagnostics used for systems that are not necessarily spatially resolved (e.g., luminous infrared galaxies; for which many excellent reports can be found in the present proceedings issue). To continue making progress in the era of *SPICA*, while improving upon sensitivity is a must, particular attention to the spatial integrity and fidelity of the data must also be drawn to achieve the full/extra success.

Support for this work was provided by NASA through an award issued by JPL/Caltech, by the Japan Society for the Promotion of Science through an FY2013 long-term invitation fellowship program, by the Belgian Federal Science Policy Office via the PRODEX Programme of ESA, and the Polish NCN through a grant 2011/01/B/ST9/02031.

REFERENCES

Bachiller, R., Huggins, P. J., Cox, P., & Forveille, T. 1993, A&A, 267, 177
Frew, D. J. 2008, Ph.D. Thesis, Macquarie University
Grevesse, N., Asplund, M., Sauval, A. J., & Scott, P. 2010, Ap&SS, 328, 179
Gruendl, R. A., et al. 2006, ApJ, 653, 339
Hiriart, D. 2005, A&A, 187, 181
Kastner, J. H., et al. 2003, ApJL, 591, L37

— 2012, AJ, 144, 58
Liu, X.-W., et al. 2001, MNRAS, 323, 343
Liu, Y., Liu, X.-W., Barlow, M. J., & Luo, S.-G. 2004a, MNRAS, 353, 1251
Liu, Y., Liu, X.-W., Luo, S.-G., & Barlow, M. J. 2004b, MNRAS, 353, 1231
Mavromatakis, F., Papamastorakis, J., & Paleologou, E. V. 2001, A&A, 374, 280
Peimbert, M., & Torres-Peimbert, S. 1983, in Planetary Nebulae, edited by D. R. Flower, 233
Phillips, J. P., Ramos-Larios, G., & Guerrero, M. A. 2011, MNRAS, 415, 513
Pilbratt, G. L., et al. 2010, A&A, 518, L1
Sahai, R., Morris, M. R., & Villar, G. G. 2011, AJ, 141, 134
Schwarz, H. E., & Monteiro, H. 2006, ApJ, 648, 430
Ueta, T., et al. 2014, A&A, submitted
Vamvatira-Nakou, C., et al. 2013, A&A, 557, A20
Vassiliadis, E., & Wood, P. R. 1994, ApJS, 92, 125
Volk, K., & Kwok, S. 1988, ApJ, 331, 435